Experimental Analysis on Local Buckling of GFRP-Foam Sandwich Pipe Under Axial Compressive Loading

CHEN Li[1], *CHEN Li*[2*], *PAN Darong*[1*], *ZHAO Qilin*[3], *NIU Longlong*[1]

1. School of Architecture Engineering, Nanjing Institute of Technology, Nanjing 211167, P.R. China;
2. Engineering Research Center of Safety and Protection of Explosion & Impact of Ministry of Education, Southeast University, Nanjing 211189, P.R. China;
3. School of Mechanical and Power Engineering, Nanjing Tech University, Nanjing 211816, P.R. China

(Received 27 October 2019; revised 13 January 2020; accepted 19 January 2020)

Abstract: To find out the local buckling behaviors of glass fiber reinforced plastic (GFRP)-foam sandwich pipe suffering axial loading, a series of quasi-static axial compression tests are carried out in the laboratory. Comparing with the test data, systematic numerical analysis on the local buckling behavior of this sandwich pipe is also conducted, and the buckling failure mechanism is revealed. The influences of the key parameters on bearing capacity of the sandwich structure are discussed. Test and numerical results show that the local buckling failure of the GFRP-foam sandwich pipe is dominated basically by two typical modes, i.e., the conjoint buckling and the layered buckling. Local buckling at the end, shear failure at the end and interface peeling failure are less efficient than the local buckling failure at the middle height, and ought to be restrained by appropriate structural measures. The local buckling bearing capacity increases linearly with the core density of the sandwich pipe structure. When the core density is relatively high (higher than 0.05 g/cm^3), the effect of increasing the core density on improving the bearing efficiency is less on the specimens with a large ratio of the wall thickness to the radius than on those with a small one. Local layered buckling is another failure mode with lower bearing efficiency than the local conjoint buckling, and it can be restrained by increasing the core density to ensure the cooperation of the inner and the outer GFRP surface layer. The bearing capacity of the GFRP-foam sandwich pipe increases with the height-diameter ratio; however, the bearing efficiency decreases with this parameter.

Key words: sandwich pipe; polyurethane foam; glass fiber reinforced plastic (GFRP); local buckling; axial compression

CLC number: TU33$^+$3 **Document code:** A **Article ID:** 1005-1120(2020)01-0129-14

0 Introduction

Thin-walled fiber reinforced plastic (FRP) structures with good bearing efficiency have been widely used in the civil engineering fields, such as wharf support columns, transmission poles, reinforced pipe piles and so on, which provide a new choice for the support equipment in emergency repairing[1-3]. However, compared with metal materials, FRP has weaker impact resistance and lower stiffness with equal volume[4-5]. Because the elastic modulus of FRP materials is relatively low, the local buckling caused by axial compression is the main failure mode of these structures[6]. If the local buckling is reduced by increasing the thickness of FRP wall, the advantages of light weight and high strength might not be exhausted, which wastes materials, increases the self-weight of the structure and increases the cost of use. Using the sandwich form can not only effectively improve the structural stability of thin-walled FRP structures, but also reduce the weight[7]. In addition, due to the energy absorp-

*Corresponding authors, E-mail addresses: li.chen@seu.edu.cn; pandarong@msn.com.

How to cite this article: CHEN Li, CHEN Li, PAN Darong, et al. Experimental analysis on local buckling of GFRP-foam sandwich pipe under axial compressive loading[J]. Transactions of Nanjing University of Aeronautics and Astronautics, 2020, 37(1):129-142.
http://dx.doi.org/10.16356/j.1005-1120.2020.01.012

tion characteristic of foam materials, the sandwich form can also improve the performances of thin-walled FRP structures in such aspects as aseismic, antiknock, etc.[8-9].

To study the buckling behaviors of the sandwich pipe structure suffering axial compression, Liu et al.[10] compared the buckling modes and the structural bearing efficiencies of the pipes with a single material and those with the cavity filled by foam material. Numerical simulation showed that the buckling capacity and efficiency of thin-walled pipes could be improved by filling with foam materials. Walker and Smith[11] studied the optimization method of sandwich composite pipe. The wall of the composite pipe is of a sandwich structure formed by FRP wall and low density core layer. The optimization took the load and the cost as the control indexes, the fiber orientation of the wall, the thickness of the wall and the core layer as the optimization variables, and the member weight as the optimization objective. It was announced that the composite sandwich pipe could meet the requirements of improving the bearing efficiency and controlling the cost more easily. Li et al.[12-13] thus proposed a FRP-foam sandwich pipe instead of the conventional thin-walled FRP pipe to bear axial loads, so as to use the geometric stiffness to make up the material stiffness, and to give full play to the strength of FRP. Moreover, the axial performance of the sandwich pipe reinforced by stiffeners was studied, and the advantages of this kind of structure were verified. Yet since the stiffeners need to be manufactured separately, the manufacturing process is relatively complicated.

The FRP-foam sandwich pipe (without stiffeners) has better axial bearing capacity than homogeneous thin-walled FRP pipe and the FRP pipe with the cavity filled core. Moreover, compared with the sandwich pipe reinforced by stiffeners, it has the convenience in manufacturing process. Thus, this paper reports a series of axial loading tests on the glass fiber reinforced plastic (GFRP)-foam sandwich pipe, i.e. polyurethane foam sandwiched by GFRP, as well as the fine numerical simulation and parameter discussions that reveal the buckling characteristics of the sandwich structure under axial compressive loading, which provide a basis to optimize the engineering design of FRP-foam sandwich pipe structure.

1 Local Buckling Test

1.1 Preparation of the specimen

The test specimens of GFRP-foam sandwich pipe are manufactured by an integral casting process[14]. The manufacture process includes the following steps: First, using the glass fiber prepreg to manufacture the GFRP tubes. The GFRP tubes are manufactured by the hand lay-up process, with the glass fiber plies of [0°/90°]. Second, two GFRP tubes with different diameters and the same height are selected as the inner and outer walls of the sandwich pipe, and are fixed. Third, the polyurethane glue is poured into the gap between the inner and outer thin-walled tubes. After it foams, cures and cools, the GFRP-foam sandwich pipe is obtained.

There are three types of specimens in the loading test: The homogeneous thin-walled GFRP pipes which is denoted as SGP, the GFRP-foam sandwich pipes without the interface between the surfaces and the core being treated, and the sandwich pipes with the interface being treated, which are denoted as SGPP. The way to treat the interface is to roughen the inter surface of the outer tube and the outer surface of the inner tube before pouring the glue, and then smear high strength epoxy adhesive on them. The detailed parameters of the pipe specimens for test are listed in Table 1 and shown in Fig. 1 for clarity.

The density of foam core layer is controlled by the mass ratio of white material, black material and blowing agent during pouring. Because the density of polyurethane foam is affected by many factors, the densities of foams with the same raw materials would also be different, and should be measured accurately for each actual specimen. The core weight is obtained by subtracting the weight of the inner and outer walls from the total weight of the sandwich pipe measured, and the core density is obtained by dividing the mass with the volume of the core layer.

Table 1 Parameters of the pipe specimens

Label	Inner diameter of the inner tube×thickness/(mm×mm)	Inner diameter of the outer tube×thickness/(mm×mm)	Core thickness/mm	Core density/($g \cdot cm^{-3}$)	Effective length/mm
SGP63-1	63×1	—	—	—	190
SGP63-2	63×1	—	—	—	136
SGP63-3	63×1	—	—	—	137
SGP63-4	63×1	—	—	—	138
SGP63-5	63×1	—	—	—	296
SGP78-1	78.4×1	—	—	—	280
SGPP35-1	35×1	78.4×1	20.7	0.090	296
SGPP35-2	35×1	78.4×1	20.7	0.090	274
SGPP52-1	52×1	78.4×1	12.2	0.099	245
SGPP52-2	52×1	78.4×1	12.2	0.091	284
SGPP52-3	52×1	78.4×1	12.2	0.097	262
SGPP63-1	63×1	78.4×1	6.7	0.254	214
SGPP63-2	63×1	78.4×1	6.7	0.256	273
SGPP63-3	63×1	78.4×1	6.7	0.181	324
SGPP63-4	63×1	78.4×1	6.7	0.165	280
SGPP63-5	63×1	78.4×1	6.7	0.395	277
SGPP63-6	63×1	78.4×1	6.7	0.452	277

SGP63-1: Short GFRP Poles 63(inner diameter)-1(order number)

SGPP52-1: Short GFRP-PUR Poles 52(inner diameter)-1(order number)

For end-unconstrained specimen, effective length refers to the actual length of the specimen; for end-constrained specimen, effective length refers to the length between the end constraint devices.

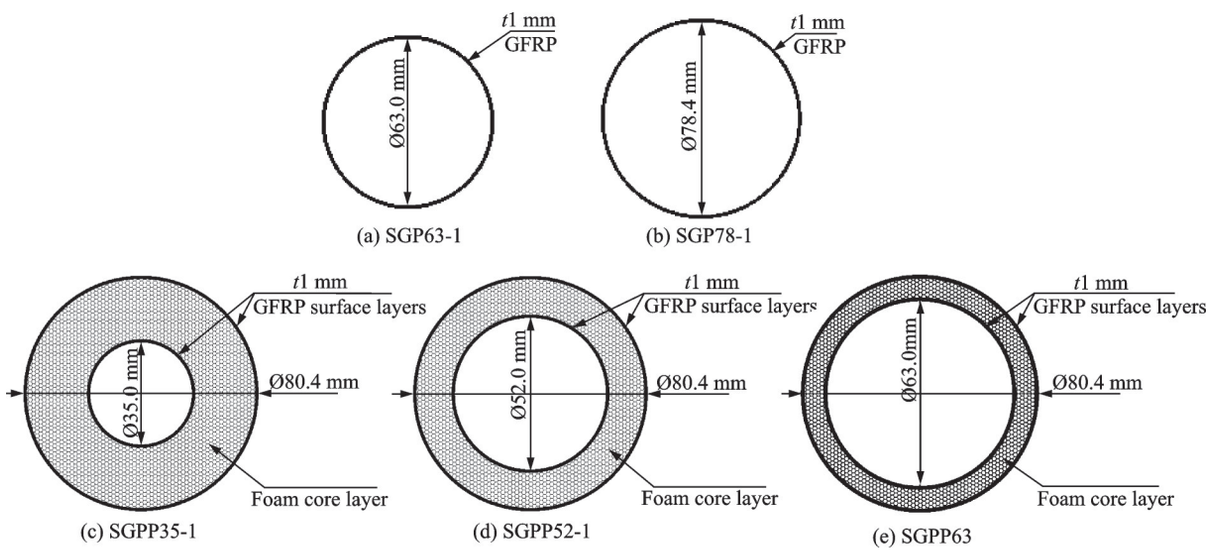

Fig.1 Sectional dimension drawing of the specimens

1.2 Determination of the material mechanical parameters

The density of the polyurethane matrix by material property test is 1.0 g/cm^3, the elastic modulus is 2.09 GPa, Poisson's ratio is 0.362, and the shear modulus is 0.767 GPa, calculated from the relationship among the shear modulus, elastic modulus and Poisson's ratio of isotropic material, namely $G=\frac{E}{2(1+\nu)}$. The strains of the pipe specimen walls are measured in the previous tests, showing that the ultimate strains of the pipe specimen walls at local buckling are less than 18 000 με. In contrast with the ma-

terial property test results, it is shown that under this strain, the polyurethane material can be considered as linear elastic. The mechanical parameters of polyurethane foam are calculated according to its density by the formula proposed by Lu et al.[15], as shown in Table 2.

Table 2 Mechanical parameters of the polyurethane foam with different densities

Density of the foam/ ($g \cdot cm^{-3}$)	Elastic modulus/GPa	Shear modulus/ GPa	Poisson's ratio
0.01	0.007	0.003	0.385
0.05	0.037	0.013	0.385
0.10	0.079	0.028	0.385
0.15	0.125	0.045	0.384
0.20	0.177	0.064	0.384
0.25	0.236	0.085	0.385
0.090	0.070	0.025	0.385
0.180	0.156	0.056	0.384
0.165	0.140	0.051	0.384
0.395	0.454	0.164	0.387
0.452	0.562	0.202	0.389

The basic mechanical parameters of the GFRP with [0°/90°] ply obtained by material property test are shown in Table 3, where E_x and E_y indicate the elastic modulus in the longitudinal and the lateral direction of the GFRP, respectively; ν_{xy}, G_{xy} and τ_{xy} indicate the in-plane Poison's ratio, in-plane shear modulus and in-plane shear strength of the GFRP, respectively.

Table 3 Mechanical parameters of GFRP obtained by material test

Mechanical parameter	E_x/ GPa	E_y/ GPa	ν_{xy}	G_{xy}/ GPa	τ_{xy}/ MPa
Average value	18.0	18.0	0.170	1.2	54.7

1.3 Test scheme

The specimens are monotonically compressed[16] on a universal material testing machine. The thin-walled GFRP pipe of SGP series and the GFRP-foam sandwich pipe of SGPP series are transversely constrained both inside and outside the ends. The end constraint device is shown in Fig. 2. The inner diameter of the hoop is the same as the outer diameter of the specimen, and the outer diameter of the lining block is the same as the inner diameter of the pipe specimen. It is advisable to keep the hoop and the lining block in close contact with the specimen without damaging it. Assembly of the loading specimens is shown in Fig. 3. The load is automatically collected by the load sensor built in the testing machine. The displacement is automatically collected by a displacement meter installed on the testing machine and in contact with the beam of the testing machine.

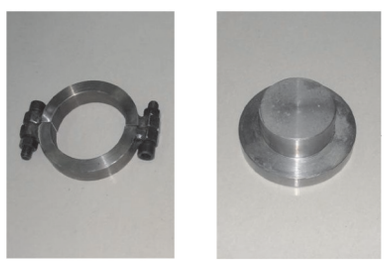

(a) Hoop (b) Lining block

Fig.2 Apparatus for end constraint

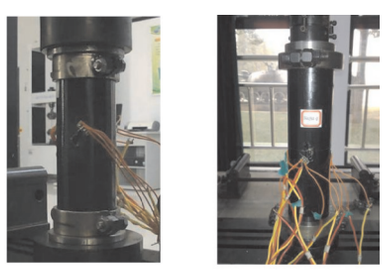

(a) Thin-walled GFRP pipe (b) Sandwich pipe

Fig.3 Assembly of the loading specimens

1.4 Test results

The failure modes of the homogeneous thin-walled GFRP pipes (SGP63-2, SGP63-3, SGP63-4, SGP63-5 and SGP78-1) are local buckling with the waveform of rhombic waves, as shown in Fig. 4.

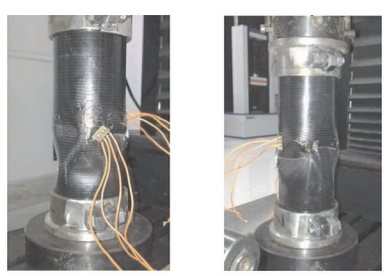

(a) Front view (b) Back view

Fig.4 Local buckling of a thin-walled GFRP pipe

The sandwich pipes (SGPP52-2, SGPP63-3, SGPP63-4, SGPP35-1 and SGPP35-2), of which the interfaces between the walls and the core layer are treated, have enough interface bonding strength to ensure the surface layer and the core layer to bear force together. When the core layer is thicker and its density is lower, the local buckling of the sandwich pipe is mainly in the form of local layered buckling (SGPP52-2, SGPP35-1, SGPP35-2). The typical failure process is that when the axial load reaches the critical value, the specimen suddenly buckles. Irregular concave-convex waves and longitudinal cracks caused by buckling appear in the middle of the specimen, and no transverse cracks are found, as shown in Fig.5(a). After cutting the specimen longitudinally, no buckling marks are found in the inner wall, as shown in Fig.5(b). It shows that only the outer wall buckles, while the inner wall does not buckle. This buckling form can be called local layered buckling.

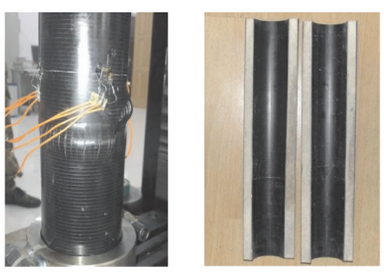

(a) Appearance of the outer wall (b) Appearance of the inner wall

Fig.5 Local layered buckling of GFRP-foam sandwich pipe

The buckling waveforms of the sandwich specimens in local layered buckling are different from those of homogeneous thin-walled GFRP specimens. They are similar to axisymmetric waves, i.e. the longitudinal waveforms are convex and concave, and the circumferential waveforms are circular, but it is difficult to obtain a standard circular wave. The uncertainty of buckling waveforms of sandwich pipes is due to the sensitivity of local buckling waveforms, and the buckling waveforms of sandwich pipes always appear first in the parts with weak mechanical properties or high stress. Since the inner and outer walls have the same thickness and the inner wall radius is smaller, the buckling of the outer wall always occurs first when local layered buckling occurs.

When the core layer of the sandwich pipe is thin and its density is high, the local conjoint buckling is the main form of the local buckling of the sandwich pipe (SGPP63-3, SGPP63-4). The typical failure process is that the specimen has no obvious deformation during the whole loading process. When the load reaches its critical value, the specimen suddenly breaks down. A complete circumferential wave crest and longitudinal cracks caused by buckling appear in the middle of the specimen, and no transverse crack is found, as shown in Fig.6(a). The buckling shape should be determined as axisymmetric waves. After cutting the specimen longitudinally, it is found that there are also buckling damage marks at the position of the inner wall corresponding to the buckling position of the outer wall, as shown in Fig.6(b). This indicates that the inner and outer walls buckle simultaneously, which can be called local conjoint buckling.

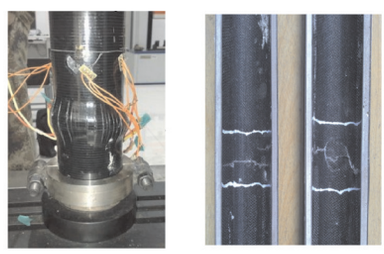

(a) Appearance of the outer wall of the damaged specimen (b) Appearance of the inner wall of the damaged specimen

Fig.6 Local conjoint buckling of GFRP-foam sandwich pipe

In addition, there are some local structural failure forms. When the ends are unconstrained (SGP63-1), the thin-walled GFRP pipes are prone to buckle at the ends, as shown in Fig.7. When the ends are constrained too tightly (SGPP52-3), the sandwich pipes are prone to shear failure at the ends, as shown in Fig.8. Sandwich pipes whose in-

terfaces between the walls and the core layers are not treated (SGPP52-1, SGPP63-1, SGPP63-2, SGPP63-5, SGPP63-6), are easy to break off between the walls and the core layer during the compression. The surfaces of the stripped walls are very smooth, and there is no residual foam material. There is no mark of buckling failure in the inner walls, as shown in Fig.9. The failure reason is that the interfaces between the outer walls and the core layers are not firmly bonded. The interfaces peel off under axial loading, and then the surface and core layers of the sandwich pipe walls could not bear force synergistically. The outer walls could not get enough lateral support, so that the individual buckling of the outer walls occurs ultimately. All these three failure forms occur before the local buckling at the middle part, which indicates that the corresponding ultimate loads are lower than the critical buckling load, and these failure forms are less effective than local buckling. They could be suppressed by taking corresponding structural measures.

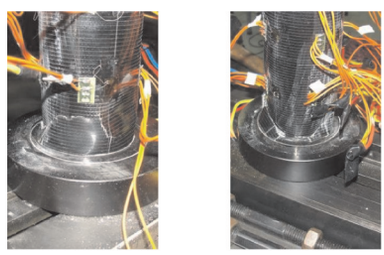

(a) Front view (b) Back view

Fig.7 End buckling of unconstrained FRP thin-walled pipe

(a) Appearance of the outer wall of the damaged specimen (b) Appearance of the inner wall of the damaged specimen

Fig.8 Shear crack at the end of the GFRP-foam sandwich pipe caused by the excessively tight steel hoop

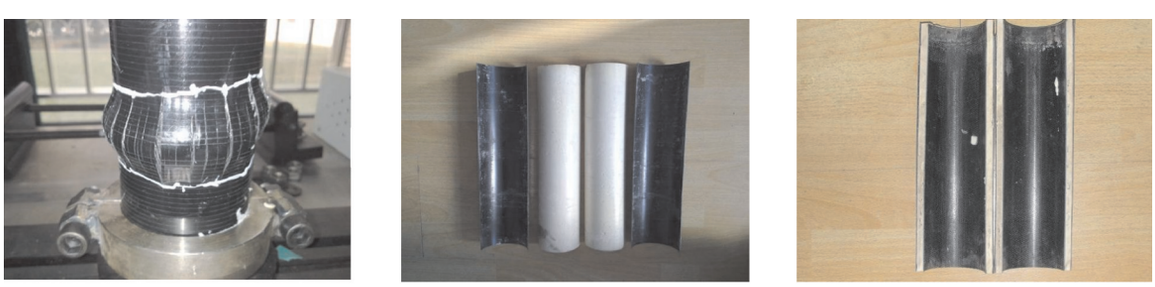

(a) Appearance of the outer wall of the damaged specimen (b) Peeling surface between the outer layer and the core layer after the failure of the specimen (c) Appearance of the inner wall of the damaged specimen

Fig.9 Peeling failure at the interface of the GFRP-foam sandwich pipe

The test results of all specimens are listed in Table 4, where n and m represent the number of the circumferential waves and the axial half waves at buckling, respectively. It can be found that the local buckling waveforms of sandwich pipes are mainly axisymmetric waves, while those of thin-walled GFRP pipes are mainly rhombic waves. The ultimate loads of the specimens failed by interface peeling are relatively small, indicating that the interface peeling is a more effective failure mode than the local buckling. After interfacial roughening and gluing treatment, the failure mode of sandwich pipes changes to local conjoint buckling, and their ultimate loads are obviously increased. To obtain better interface bonding effect, Z-pins[17] or stiffeners can be used to enhance the interface. The displacement-load curves of the pipe specimens are further discussed with numerical analysis.

Table 4 Results for compression tests of the pipe specimens

Label	Critical load/kN	Failure form	Buckling mode	$2n\times m$
SGP63-1	15.229	End local buckling (Abnormal)	Rhombic waves	4×1
SGP63-2	35.184	Local buckling	Rhombic waves	8×2
SGP63-3	36.165	Local buckling	Rhombic waves	8×2
SGP63-4	32.857	Local buckling	Rhombic waves	8×2
SGP63-5	34.063	Local buckling	Rhombic waves	4×1
SGP78-1	32.0	Local buckling	Rhombic waves	4×1
SGPP35-1	68.936	Local layered buckling	Axisymmetric waves	0×1
SGPP35-2	64.910	Local layered buckling	Axisymmetric waves	0×1
SGPP52-1	86.935	Interface peeling (abnormal)	—	—
SGPP52-2	108.514	Local layered buckling	Axisymmetric waves	0×1
SGPP52-3	92.550	Shear failure at the end constraint (abnormal)	—	—
SGPP63-1	150.386	Interface peeling (abnormal)	—	—
SGPP63-2	153.860	Interface peeling (abnormal)	—	—
SGPP63-3	137.372	Local conjoint buckling	Axisymmetric waves	0×1
SGPP63-4	140	Local conjoint buckling	Axisymmetric waves	0×1
SGPP63-5	157.0	Interface peeling (abnormal)	—	—
SGPP63-6	153.0	Interface peeling (abnormal)	—	—

2 FE Models for Local Buckling Analysis

2.1 Construction of the FE Models

2.1.1 Model for eigenvalue buckling analysis

The general finite element analysis software ANSYS is used to analyze the buckling of pipe specimens under axial compression. Firstly, the eigenvalue buckling analysis is adopted to analyze the local buckling of the axially compressed specimens, without considering the initial defects of the members. For both the GFRP layers and the foam core, Solid45 3D solid element is adopted. It was assumed that the deformation between the GFRP walls and the foam core of the sandwich pipes is coordinated, and the peeling between them is not considered. The GFRP elements and the foam core elements shear nodes on the contact surface. In the preliminary analysis, it is found that the mesh size has great influence on the calculation results. By comparing the differences between the calculated results, sufficiently fine mesh sizes are selected. The translational degrees of freedom of the nodes located at the upper and the lower end faces of the specimen are coupled respectively. In this way, the displacement of all the nodes of the upper end face or the lower end face is the same when loading, so that the surface layer and the core layer had the same axial strain. Hinge constraints are applied at both ends of the specimen and a compression force is applied on the upper surface. The mechanical parameters in Table 3 are adopted as those of the GFRP material. According to the test results, the foam core does not enter the plastic state when buckling occurs. The mechanical parameters of the foam core are shown in Table 2.

2.1.2 Model for nonlinear buckling analysis

Based on the FE model established above, initial imperfection is applied according to the first buckling mode obtained from eigenvalue buckling analysis to stimulate the buckling effect. The load of

the same magnitude as the eigenvalue buckling load is applied to the specimen model by slope loading. The arc length method is used to execute the nonlinear buckling analysis. The actual specimen might have both initial geometric defects and initial mechanical defects, which are considered as a unified geometric defect uniformity. By trial calculation, the analytical results when the initial geometric defect is $1.5t$ are in relatively good agreement with the test results, where t is the total wall thickness of the thin-walled GFRP pipe or the sandwich pipe.

2.2 Verification of the model

2.2.1 Comparison of buckling mode results

Fig. 10 shows the typical buckling mode of the sandwich pipe specimens obtained by FE analysis. The left and right figures corresponding to each specimen show respectively the whole deformed specimen and the profile when cutting the specimen along its central axis. The deformation of the outer and inner walls of the buckled specimens can be seen in these figures, so as to judge whether the inner and outer walls have both buckled. Table 5 lists the data obtained in the tests and the FE simulations, in which $P_{cr,Ex}$, $P_{cr,Linear}$ and $P_{cr,Nonlinear}$ are the tested, eigenvalue buckling analysis and nonlinear buckling analysis results of critical buckling load, respectively. $2n$ is the annular half-wave number and m is the longitudinal half-wave number.

For all the specimens, the buckling forms (local layered buckling or local conjoint buckling) obtained by numerical simulation are consistent with the test results, but the buckling waveforms are quite different. This is because the boundary conditions set in ANSYS are very difficult to be exactly the same with that in the experiment, and the specimens have initial defects. Meanwhile, the local buckling modal is very sensitive to the conditions and is easily affected. Thus it cannot be inferred that the accordance between the other results obtained by the two approaches is meaningless[18]. This can also be proved in the sensitivity analysis of local buckling modes carried out below.

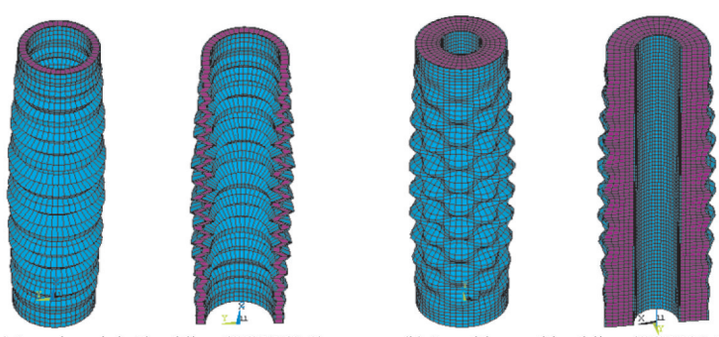

(a) Local conjoint buckling (SGPP63-3) (b) Local layered buckling (SGPP35-2)

Fig. 10 Two typical local buckling modes of sandwich pipe calculated by FE analysis

Table 5 Comparison of results between test and FE analysis

Label	Buckling mode by test		Buckling mode by FEM analysis		Result of P_{cr}					
	Buckling form	$2n\times m$	Buckling form	$2n\times m$	$P_{cr,Ex}$	$P_{cr,Linear}$	$P_{cr,Nonlinear}$	$\frac{P_{cr,Linear}}{P_{cr,Ex}}$	$\frac{P_{cr,Nonlinear}}{P_{cr,Ex}}$	$\frac{P_{cr,Nonlinear}}{P_{cr,Linear}}$
SGP63-2	Local buckling	8×2	Local buckling	10×8	35.184	45.740	32.425	1.300	0.922	0.709
SGP63-3	Local buckling	8×2	Local buckling	10×8	36.165	45.866	32.310	1.268	0.893	0.704
SGP63-4	Local buckling	8×2	Local buckling	10×8	32.857	45.866	32.206	1.396	0.980	0.702
SGP63-5	Local buckling	4×1	Local buckling	10×16	34.063	46.095	31.379	1.353	0.921	0.681
SGPP35-1	Local layered buckling	0×1	Local layered buckling	10×22	68.936	74.036	50.800	1.074	0.707	0.658
SGPP35-2	Local layered buckling	0×1	Local layered buckling	10×21	64.910	74.949	51.999	1.155	0.801	0.694
SGPP52-2	Local layered buckling	0×1	Local layered buckling	0×41	108.514	135.079	87.383	1.245	0.805	0.647
SGPP63-3	Local conjoint buckling	0×1	Local conjoint buckling	0×119	137.372	169.541	133.412	1.234	0.971	0.787
SGPP63-4	Local conjoint buckling	0×1	Local conjoint buckling	0×91	140.0	166.095	133.376	1.186	0.953	0.803

2.2.2 Comparison of displacement-load relations

The displacement-load curves of specimens with different buckling forms, which are obtained by FE analysis and test respectively, are compared in Fig.11. The measured displacement contains the rigid body movement between the displacement meter and the test fixtures. This is the reason why the initial zero drifts of the measured displacement-load curves exist, namely why the measured displacement at small loads is quite large and different from the numerical value. Considering the initial geometric defects, the displacement-load relationships at the ends of the specimens obtained by nonlinear buckling analysis are basically linear before buckling, which is consistent with the test results. At the same time, the slopes of the curves obtained from FE analysis and the test are slightly different. It is because that the GFRP tubes are prepared by hand lay-up process, while the foam core layers are cast by manual foaming, which can induce a little discreteness. If the initial zero drift of the tested displacement is excluded, the displacement-load curve obtained by the FE analysis is in comparatively good agreement with the test data.

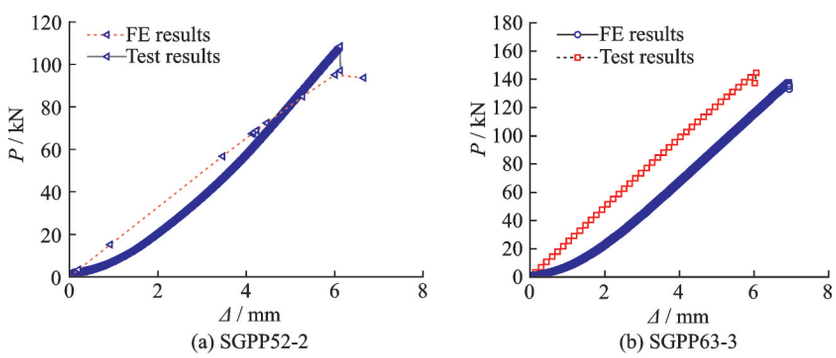

Fig.11 Comparison of typical end displacement-load curves with different buckling forms

2.2.3 Comparison of buckling loads

Comparison of critical buckling loads is presented in Table 4, in which $P_{\mathrm{cr,Ex}}$, $P_{\mathrm{cr,Linear}}$ and $P_{\mathrm{cr,Nonlinear}}$ represent the results of test, eigenvalue buckling analysis (linear buckling analysis) and nonlinear buckling analysis, respectively.

The maximum and minimum values of $\frac{P_{\mathrm{cr,Linear}}}{P_{\mathrm{cr,Ex}}}$ are 1.396 and 1.074, respectively, and the average value is 1.246. The actual members have large geometric and material defects, and the constraints and loading conditions are inconsistent with the ideal state, which cause that the results of linear buckling analysis much larger than the actual buckling loads.

The maximum and minimum values of $\frac{P_{\mathrm{cr,Nonlinear}}}{P_{\mathrm{cr,Ex}}}$ are 0.980 and 0.707, respectively. The average value is 0.884 and the standard deviation is 0.087. This indicates that in general, the adopted initial geometric defect of $1.5t$ for the nonlinear buckling analysis is larger than the actual defects, and the critical buckling loads obtained by the analysis tend to be conservative.

Although the initial geometric defects of the specimens are uniform in finite element calculation, they are not the same for different specimens. The average value of $\frac{P_{\mathrm{cr,Nonlinear}}}{P_{\mathrm{cr,Linear}}}$ is 0.709 and the standard deviation is 0.047. The standard deviation is 6.7% of the average. The discreteness of $\frac{P_{\mathrm{cr,Nonlinear}}}{P_{\mathrm{cr,Linear}}}$ shows that the influence of specimen defects on local buckling load is uncertain and may be related to many factors, such as the length, the ratio of the wall thickness to the radius, the core thickness and the material parameters. Therefore, the local buckling loads obtained from the eigenvalue buckling analysis will be taken as the research object, to eliminate the influence of defects on the local buckling loads.

3 FE Analysis of Local Buckling Behavior of the Sandwich Pipes

3.1 Expanded specimens and results

Eigenvalue buckling analysis is applied to discuss the local buckling behaviors of GFRP-foam sandwich pipes. The 34 expanded specimens with regularly varying parameters are designed and analyzed. The middle diameter of the specimens is all 60 mm, and the thickness of the walls is all 1 mm. In addition to the two forms of local buckling mentioned above, some extended specimens fail with the form of overall buckling in the FE analysis.

The related parameters and corresponding calculation results are shown in Table 6. It is found that the buckling forms of specimens with the core thickness 4 mm and the effective length 300 mm or 420 mm are local conjoint buckling. The buckling

Table 6 Parameters of the expanded GFRP-foam specimen and corresponding calculated results in the eigenvalue buckling analysis

Label	Effective length/mm	Height-diameter ratio	Surface layer thickness/mm	Core layer thickness/mm	Core layer density/(g•cm^{-3})	Buckling form	$2n\times m$	P_{cr}/kN	Bearing efficiency/(kN•kg^{-1})
CSGPP-1	300	5	1	4	0.01	Local conjoint buckling	10×22	90.01	482.35
CSGPP-2	300	5	1	4	0.05	Local conjoint buckling	10×31	105.13	537.31
CSGPP-3	300	5	1	4	0.1	Local conjoint buckling	8×35	122.08	589.85
CSGPP-4	300	5	1	4	0.15	Local conjoint buckling	0×47	137.20	628.55
CSGPP-5	300	5	1	4	0.2	Local conjoint buckling	0×50	152.35	663.56
CSGPP-6	300	5	1	4	0.25	Local conjoint buckling	0×97	166.31	690.37
CSGPP-7	300	5	1	20	0.01	Local layered buckling	12×21	77.77	397.49
CSGPP-8	300	5	1	20	0.05	Local layered buckling	8×32	106.53	442.23
CSGPP-9	300	5	1	20	0.1	Local layered buckling	0×40	133.94	450.29
CSGPP-10	300	5	1	20	0.15	Local layered buckling	0×46	159.60	450.84
CSGPP-11	300	5	1	20	0.2	Local layered buckling	0×60	181.71	442.61
CSGPP-12	300	5	1	20	0.25	Local layered buckling	0×66	204.19	437.16
CSGPP-13	420	7	1	4	0.01	Local conjoint buckling	10×25	99.90	382.38
CSGPP-14	420	7	1	4	0.05	Local conjoint buckling	10×34	108.32	395.43
CSGPP-15	420	7	1	4	0.1	Local conjoint buckling	10×37	127.59	440.35
CSGPP-16	420	7	1	4	0.15	Local conjoint buckling	8×42	145.40	475.80
CSGPP-17	420	7	1	4	0.2	Local conjoint buckling	8×47	163.84	509.72
CSGPP-18	420	7	1	4	0.25	Local conjoint buckling	4×52	182.57	541.35
CSGPP-19	420	7	1	20	0.01	Local layered buckling	12×25	79.61	290.62
CSGPP-20	420	7	1	20	0.05	Local layered buckling	10×38	111.24	329.84
CSGPP-21	420	7	1	20	0.1	Local layered buckling	0×47	143.70	345.09
CSGPP-22	420	7	1	20	0.15	Local layered buckling	0×51	173.78	350.65
CSGPP-23	420	7	1	20	0.2	Local layered buckling	0×49	205.54	357.61
CSGPP-24	420	7	1	20	0.25	Local layered buckling	0×47	237.55	363.26
CSGPP-25	540	9	1	4	0.25	Local conjoint buckling	6×53	195.69	451.29
CSGPP-26	600	10	1	4	0.25	Local conjoint buckling	6×53	200.02	415.15
CSGPP-27	660	11	1	4	0.25	Local conjoint buckling	8×42	203.83	384.61
CSGPP-28	670	11.2	1	4	0.25	Local conjoint buckling	8×51	204.47	380.04
CSGPP-29	680	11.3	1	4	0.25	Total buckling	—	204.40	374.34
CSGPP-30	540	9	1	20	0.01	Local layered buckling	10×33	90.01	255.56
CSGPP-31	660	11	1	20	0.01	Local layered buckling	10×35	92.46	214.81
CSGPP-32	900	15	1	20	0.01	Local layered buckling	10×39	97.60	166.27
CSGPP-33	1140	19	1	20	0.01	Local layered buckling	10×41	102.98	138.51
CSGPP-34	1260	21	1	20	0.01	Total buckling	—	89.35	108.73

forms of the specimens with core thickness 20 mm and the effective length 300 mm or 420 mm are all local layered buckling. Thus, it is noted that the thicker the core layer is, the more difficult it is for the inner and outer walls of the sandwich pipe to deform coordinately, and the greater the possibility of local layered buckling is. This is consistent with the test data.

3.2 Effect of core layer parameters on bearing capacity and bearing efficiency of the sandwich pipes

The influence curves of core density on local buckling bearing capacity and bearing efficiency are presented in Figs.12 and 13, respectively, in which the bearing efficiency is obtained by dividing the bearing capacity with the mass of the specimen. In the figures, h_2 denotes the thickness of the core layer and L the effective length of the specimen. As shown in Fig.12, the local buckling bearing capacity increases with the core density approximately in a linear form. As shown in Fig.13, when the core density changes from 0.01 g/cm^3 to 0.25 g/cm^3, the bearing efficiency of the specimens with h_2=4 mm increases continuously, and the increasing trend of the bearing efficiency of the specimens with h_2=20 mm slows down after the core density reaches 0.05 g/cm^3. Especially for the specimens with h_2=20 mm and L=300 mm, the bearing capacity decreases after the core density reaches 0.05 g/cm^3. It reveals that when the core layer density is higher than 0.05 g/cm^3, the effect of increasing the core layer density on improving the bearing efficiency is less obvious for the specimen with thick core layer than for those with thin core layer.

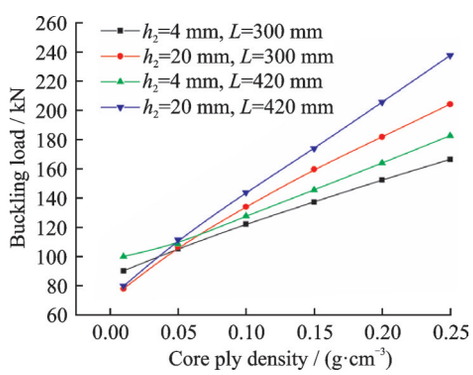

Fig.12 Effect of core density on local buckling bearing capacity of the sandwich pipes

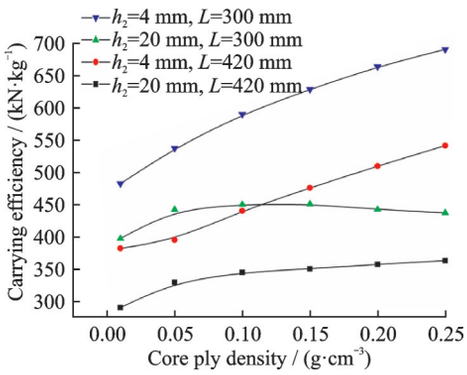

Fig.13 Effect of core density on local buckling bearing efficiency of the sandwich pipes

The bearing efficiency of the specimens with h_2=4 mm is higher than that of the specimens with h_2=20 mm. This is because that when the core layer is too thick, the inner and outer walls of the specimen are not easy to bear load coordinately, which will result in the layered buckling of the specimen. At this time, the core layer part far from the outer wall is not easy to play a supporting role to the outer wall. Therefore, an excessive thick core layer of sandwich pipe may result in the reduction of bearing efficiency. When the core density is larger than 0.05 g/cm^3, the bearing capacity of the specimens with h_2=4 mm is less than those with h_2=20 mm. When the core density is smaller than 0.05 g/cm^3, the bearing capacity of the specimens with h_2=4 mm is even larger than those with h_2=20 mm. It is obvious that in the case of layered buckling, increasing the thickness of the core will reduce the bearing efficiency, and even reduce the bearing capacity of the member when the density of the core layer is small. The specimens with h_2=20 mm and those with h_2=4 mm fail in the forms of layered buckling and conjoint buckling, respectively. Fig. 13 shows that the bearing efficiency of the former is lower than that of the latter with the same length. The local layered buckling is a failure form with lower bearing efficiency than the local conjoint buckling. It can be reduced by increasing the density of the core layer to ensure the coordinated work of inner and outer tube walls.

3.3 Effect of height-diameter ratio on bearing capacity and bearing efficiency of the sandwich pipes

Figs. 14 and 15 present the influences of

height-diameter ratio on local buckling bearing capacity and bearing efficiency, respectively. For the sandwich pipes of 4 mm core thickness and 0.25 g/cm^3 core density, the local buckling forms are all conjoint buckling. The local buckling bearing capacity increases with the height-diameter ratio, but the bearing efficiency decreases continuously. When the height-diameter ratio reaches 11.3, the bearing capacity suddenly decreases. It is attributed that the failure form of the specimens changes from local buckling to overall buckling. For the sandwich pipes of 20 mm core thickness and 0.01 g/cm^3 core density, the local buckling forms are all layered buckling. Similarly, the local buckling bearing capacity increases with the height-diameter ratio, and the bearing efficiency decreases continuously. When the ratio of height-diameter reaches 21, the bearing capacity suddenly decreases. It dues to that the failure mode changes from local buckling to overall buckling.

It can be found that for both local layered buckling and local conjoint buckling, the bearing capacity of the sandwich pipe increases with the height-diameter ratio. It is because the height-diameter ratios

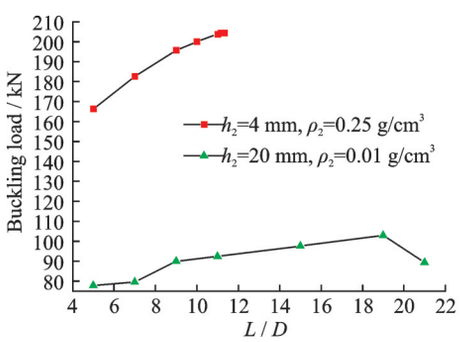

Fig.14 Effect of height-diameter ratio on local buckling bearing capacity of the sandwich pipes

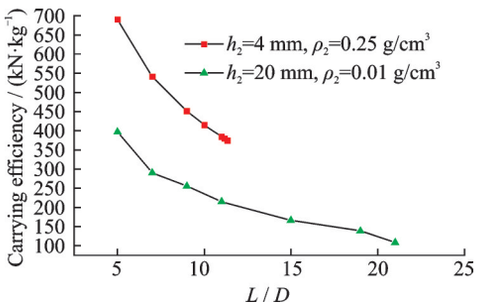

Fig.15 Effect of height-diameter ratio on local buckling bearing efficiency of the sandwich pipes

studied in this paper are larger than 5, and the influence of end constraint conditions is not significant. In this case, the larger the height-diameter ratio is, the smaller the diameter of the sandwich pipe is related to the height, and the thicker its wall thickness is related to the height, too. So the more difficult it is for the local buckling to occur. However, the load bearing efficiency decreases continuously with the height-diameter ratio.

3.4 Sensitivity of local buckling modes of the sandwich pipes

The sensitivity of local buckling modes (waveforms) is studied with CSGPP-1 as an example. Table 7 lists its 1st—10th order buckling loads. Although the shape of the buckling modes varies greatly, the difference of the buckling loads is not significant. The 10th buckling load is only 0.24% larger than the 1st buckling load. Similar conclusions could be obtained for the other specimens. It shows that the local buckling mode is very sensitive when the buckling load remains almost unchanged. The slight change in boundary conditions and material properties might lead to large difference in local buckling modes. However, the buckling loads might not be affected much.

Table 7 Local buckling loads of order 1—10 of CSGPP-1

Order number	1	2	3	4	5
Buckling load /kN	90.011 90	90.011 90	90.013 03	90.013 03	90.091 07
Order number	6	7	8	9	10
Buckling load /kN	90.091 07	90.093 33	90.093 33	90.224 53	90.224 53

4 Conclusions

The local buckling waveforms of the GFRP-foam sandwich pipes are mainly axisymmetric waves, while those of the thin-walled GFRP pipes are mainly rhombic waves. When the core layer of the sandwich pipe is relatively thick and its density is relatively low, local layered buckling dominates the main form of local buckling. Otherwise, local conjoint buckling is the main form. Since the inner

and outer walls have the same thickness and the inner wall radius is smaller, the outer wall always buckles first.

When the ends are unconstrained, the thin-walled GFRP pipes are prone to buckle at the ends. When the ends are constrained too tightly, the sandwich pipes are prone to shear failure at the ends. If the interfaces between the walls and the core layers are not treated, the sandwich pipes are easy to break off between the walls and the core layer during compression. All these three failure forms are less effective failure forms than local buckling in the middle part of the sandwich pipe. They should be suppressed by taking corresponding structural measures.

The local buckling modes of thin-walled GFRP pipes and the sandwich pipes are very sensitive. Except for the buckling modes (wave forms), the local buckling forms (layered buckling or conjoint buckling) of the specimens obtained by FE eigenvalue buckling analysis are in good agreement with the test results. However, the buckling loads deviate moderately from the test results, which is due to the initial defects of the actual specimens. The critical buckling loads obtained by the FE nonlinear buckling analysis considering the initial geometric defect of $1.5t$ is close to the test results, and tend to be conservative.

The local buckling bearing capacity increases with the core density, and the trend is basically linear. When the core density is higher than 0.05 g/cm^3, the effect of increasing the core density on improving the bearing efficiency is less obvious for the specimen with thicker core layer than for those with thinner core layer.

When the core layer is too thick, it is not easy for the inner and outer layers to bear load coordinately, which results in the layered buckling of the sandwich pipe. Therefore, an excessively thick core layer may result in the reduction of load bearing efficiency conversely. In the case of layered buckling, increasing the thickness of the core layer will reduce the bearing efficiency, and even reduce the bearing capacity of the sandwich pipe when the density of the core layer is low. Local layered buckling is a failure mode with lower bearing efficiency than local conjoint buckling. It can be improved by increasing core density to ensure that the inner and outer walls work in harmony.

For sandwich pipes with a height-diameter ratio more than 5, the bearing capacity increases with the height-diameter ratio, but the bearing efficiency decreases with it continuously, regardless of whether the buckling form is local layered buckling or local conjoint buckling.

References

[1] GODAT A, LÉGERON F, GAGNÉ V, et al. Use of FRP pultruded members for electricity transmission towers[J]. Composite Structures, 2013, 105(8): 408-421.

[2] LIU J, QIN M, ZHAO Q, et al. Fatigue performances of the cracked aluminum-alloy pipe repaired with a shaped CFRP patch[J]. Thin-Walled Structures, 2017, 111: 155-164.

[3] CHEN L, ZHENG K, FANG Q. Effect of strain rate on the dynamic tensile behaviour of UHMWPE fibre laminates[J]. Polymer Testing, 2017, 63: 54-64.

[4] DAVIES G A O, HITCHINGS D, ZHOU G. Impact damage and residual strengths of woven fabric glass/polyester laminates[J]. Composites Part A, 1996, 27(12): 1147-1156.

[5] ATAS C, SAYMAN O. An overall view on impact response of woven fabric composite plates[J]. Steel Construction, 2008, 82(3): 336-345.

[6] YAN G, HAN X, YAN C, et al. Buckling analysis of composite cylindrical shell under axial compression load[J]. Acta Materiae Compositae Sinica, 2014, 31(3): 781-787. (in Chinese)

[7] MEO M, VIGNJEVIC R, MARENGO G. The response of honeycomb sandwich panels under low-velocity impact loading[J]. International Journal of Mechanical Sciences, 2005,47(9): 1301-1325.

[8] JACKSON M, SHUKLA A. Performance of sandwich composites subjected to sequential impact and air blast loading[J]. Composites Part B Engineering, 2011, 42(2): 155-166.

[9] XIE Z, SU N, ZHANG L, et al. Damage propagation behavior of composite honeycomb sandwich panels under low-velocity impact[J]. Journal of Nanjing University of Aeronautics & Astronautics, 2009, 41(1): 30-35. (in Chinese)

[10] LIU S, CHEN X, CAO X, et al. Optimization of buckling-prone cylindrical shells with porous material core[J]. Engineering Mechanics, 2005, 22(1): 135-140. (in Chinese)

[11] WALKER M, SMITH R. A procedure to select the

best material combinations and optimally design composite sandwich cylindrical shells for minimum mass[J]. Materials & Design, 2006,27(2): 160-165.
[12] TAO J, LI F, ZHU R, et al. Compression properties of a novel foam-core sandwich cylinder reinforced with stiffeners[J]. Composite Structures, 2018, 206: 499-508.
[13] TAO J, LI F, SHAO F. Experimental study for in-plane compression and interfacial fracture properties of stiffened foam core sandwich structure[J]. Acta Materiae Compositae Sinica, 2018, 35(5): 1123-1130. (in Chinese)
[14] HE Y. Comparison of two moulding techniques for FRP/PUR sandwich structure[J]. Application of Engineering Plastics, 1999, 27(10): 14-15. (in Chinese)
[15] LU Z, ZHAO M. Research progress on mechanical properties of foam plastics [J]. Mechanics in Engineering, 1998, 20(2): 1-9. (in Chinese)
[16] FAN H, HONG W, SUN F, et al. Lateral compression behaviors of thin-walled equilateral triangular tubes [J]. International Journal of Steel Structures, 2015, 15(4): 785-795.
[17] CHU Q, LI Y, XIAO J, et al. Bridging effect and efficiency of partly-cured Z-pin reinforced composite laminates[J]. Transactions of Nanjing University of Aeronautics and Astronautics, 2017, 34(2): 177-187.
[18] HUR S, SON H, KWEON J, et al. Postbuckling of composite cylinders under external hydrostatic pressure[J]. Composite Structures, 2008, 86 (1/2/3): 114-124.

Acknowledgements This work was supported by the National Key R&D Program of China (No.2017YFC0405103), the Natural Science Foundation of China (No. 51978166), and the Construction System Science and Technology Guidance Project of Jiangsu (Nos.2017ZD131, 2017ZD132).

Authors Dr. **CHEN Li** received his B.S. degree in road, bridge and river-crossing engineering and Ph.D. degree in bridge and tunnel engineering from PLA University of science and technology in 2004 and 2012, respectively. He joined in Nanjing Institute of Technology in 2016. His research is focused on emergency engineering structure.

Prof. **CHEN Li** received his B.S. and Ph.D. degrees in civil engineering from PLA University of science and technology in 2003 and 2008, respectively. He joined in Southeast University in 2018, and is currently a professor at Southeast University. His research is focused on the blast resistance of civil structures.

Dr. **PAN Darong** received his B.S. degree in civil engineering and Ph.D. degree in bridge and tunnel engineering from PLA University of science and technology in 2001 and 2009, respectively. He joined in Nanjing Institute of Technology in 2014. His research is focused on composite structure and bridge structure.

Author contributions Dr. **CHEN Li** executed the experiment and wrote the manuscript. Prof. **CHEN Li** designed this paper and interpreted the results. Dr. **PAN Darong** constructed the FE model and executed the FE analysis. Prof. **ZHAO Qilin** guided the study and provided the specimens. Mr. **NIU Longlong** participated in the experiment, and contributed to the discussion and background of the study. All authors commented on the manuscript draft and approved the submission.

Competing interests The authors declare no competing interests.

(Production Editor: WANG Jing)

GFRP泡沫夹芯管轴压局部屈曲试验分析

陈 立[1], 陈 力[2], 潘大荣[1], 赵启林[3], 牛龙龙[1]

(1. 南京工程学院建筑工程学院, 南京 211167, 中国;
2. 东南大学教育部爆炸冲击安全防护工程研究中心, 南京 211189, 中国;
3. 南京工业大学机械与动力学院, 南京 211816, 中国)

摘要:为研究玻璃纤维增强塑料(Glass fiber reinforced plastic, GFRP)泡沫夹芯管轴向受压局部屈曲性能,本文开展了以聚氨酯泡沫为芯层的GFRP泡沫夹芯管的轴向受压屈曲试验,并在试验的基础上开展了局部屈曲性能数值模拟分析,得到了这种结构的屈曲破坏现象和相关参数影响规律。研究表明,GFRP泡沫夹芯圆柱壳的局部屈曲有共同屈曲和分层屈曲两种形式;端部局部屈曲、端部剪切破坏和界面剥离是比局部屈曲更低效的破坏形式,需通过构造措施来加以抑制;局部屈曲承载力随芯层密度的增加而线性增加;当芯层密度较高(大于0.05 g/cm^3)时,增加芯层密度对提高承载效率的效果对于壁厚较大的试件不如对壁厚较小的试件明显;局部分层屈曲是比局部共同屈曲承载效率更低的破坏形式,可通过提高芯层密度加以抑制,保证内外管壁协调工作;夹芯圆柱壳承载力均随高径比的增加而增加,但承载效率随高径比的增加而持续下降。

关键词:夹芯管;聚氨酯泡沫;玻璃纤维增强塑料;局部屈曲;轴向压缩